Asian Journal of Chemistry; Vol. 34, No. 4 (2022), 945-952

ASIAN JOURNAL OF CHEMISTRY

https://doi.org/10.14233/ajchem.2022.23634

Lead(II) Schiff Base Complexes: Design, Synthesis, Theoretical, Antibacterial and Docking Studies

ANUPAMA SHARMA[1], SHIVENDRA SINGH[1,2] and HARLAL SINGH[1,*]

[1]Department of Chemistry, Mody University of Science and Technology, Lakshmangarh-332311, India
[2]Department of Applied Chemistry, Amity University Madhya Pradesh, Gwalior-474 015, India

*Corresponding author: E-mail: hlsingh9@rediffmail.com

Received: 24 November 2021; *Accepted*: 11 January 2022; *Published online*: 10 March 2022; AJC-20738

This study presented the bioactive lead(II) compounds of oxazine and thiazine Schiff-bases using NMR (^{1}H, ^{13}C), FT-infrared spectroscopy, UV-visible, molar conductance, elemental analysis and molecular weight. The molecular parameters *e.g.* bond length, bond angle, HOMO/LUMO energy gap and softness/hardness was calculated by DFT-B3LYP/Lanl2dz basis set. According to the spectral data, the Schiff-base coordinated to the lead atom in bidentate mode. A theoretical DFT computational investigation was conducted to supplement the experimental data. The antibacterial activity of lead complexes against *E. coli* (–) and *S. aureus* (+) bacteria was determined by disc-diffusion method. Lead complexes of thiazine derivatives are more active than oxazine derivatives. In order to better understand the molecular interaction and binding mode of the drugs, a molecular docking study has been carried out on the protein 3q8u (NDK) from *S. aureus*. A docking investigation with the NDK protein (*S. aureus*) revealed that compound **1h** has the highest binding affinity (-8.18 Kcal/mol) among the eight ligands (**1a-h**).

Keywords: Lead(II) complexes, Schiff base, Spectral, Computational, Antibacterial, Molecular docking studies.

INTRODUCTION

Schiff bases containing sulphur, nitrogen and oxygen donor atoms are a fascinating class of organic compounds with both medicinal and non-medicinal properties that have gained popularity over the last decade [1-3]. The Schiff bases are synthesized by reacting an aldehyde/ketone with a primary amine [4]. Metal compounds containing Schiff base ligands have garnered extensive attention for their many applications in inorganic, metallo-organic and biological sciences [5,6]. They display a broad spectrum of chemical, optical and magnetic properties as a result of their modification with various ligands [7,8]. Due to their stability under a wide range of oxidative and reductive conditions, Schiff bases have been discovered to make a significant contribution to the coordination chemistry of main group/transition metals as chelating ligands [9].

Metal complexes of various geometries form when these ligands interact with metal ions and according to a literature review, these complexes may be more physiologically active, possessing antiviral, antimicrobial, anti-inflammatory, anti-cancer, antimalarial and antipyretic effects than free ligands [10-12]. Moreover, the antimicrobial/bioactive characteristics of organic ligands can be significantly affected by metal-chelation, leading to the synthesis of a large number of metal-complexes in this field [13]. Bacterial infection and resistance to a wide variety of antibacterial treatments has become an increasingly serious concern in recent years [14,15]. While various classes of antibacterial medicines are already available, the majority of pathogenic bacteria have evolved strong resistance to them [16].

To combat this grave medical concern, new antibacterial medicines must be discovered or the bioactivity of already existing antibiotics must be boosted [17]. Metal-based antibacterial compounds are being investigated as a potential new therapeutic approach for developing new antibiotic drugs that can help control and inhibit bacterial strain growth [18,19]. Additionally, molecular docking was performed, as computational aided drug development is a valuable, quick and cost-effective strategy that has been shown to be more effective than wet lab drug discovery [20]. After docking the drug-like molecule to a protein target, a scoring function is used to determine the probability that the chemical will bind to the protein

with high affinity [21]. The synthesis of lead(II) complexes containing a Schiff base generated from oxazine and thiazine is described in this article. Numerous spectroscopic techniques were employed to characterize the synthesized compounds, as well as to determine their antibacterial activity and docking studies.

EXPERIMENTAL

All chemicals and solvents were acquired and are being used in their original form from Alfa-Aesar and Aldrich. The $^1H/^{13}C$ NMR spectra of the compounds in DMSO-d_6 have been recorded on a BRUKER, 500MHz spectrometer with TMS (internal standard). The FTIR spectra were taken on a Perkin-Elmer SP-2 spectrometer (KBr). Gaussian 05 at DFT/B3LYP was used to optimize the structures of the synthesized compounds [22,23]. Melting points were determined using open glass capillaries on electrothermal melting point apparatus. *n*-Hexane/ EtOAC (1:3) was used as the eluent for TLC. The ligands were synthesized *via* condensation of aldehydes with oxazine and thiazine derivatives, as described [24].

Synthesis of Pb(II) compounds: All the Pb(II) complexes were synthesized in a similar manner. The ligands solution in ethanol (1 mmol) was mixed with $Pb(OOCCH_3)_2$ and refluxed for 3-5 h at 70-80 ºC on a waterbath. Filtration, washing with ethanol and cyclohexane and drying in a vacuum desiccator were per-formed on the precipitate.

***Bis*(2-({(6-([1,1′-biphenyl]-4-yl)-4-(4-methoxyphenyl)-2*H*-1,3-oxazin-2-yl)imino}methyl)-6-methoxyphenolate lead(II) (2a):** Yield: 70%, solid brown, m.p.: 126-128 ºC. Elemental analysis for $C_{62}H_{50}N_4O_8Pb$ (m.w.: 1186.28) calcd. (found): C, 62.77 (62.48); N, 4.72 (4.65); H, 4.25 (4.21); Pb, 17.47 (17.25). Molar conductivity: 17.4 Ω^{-1} mol^{-1} cm^2.

***Bis*(2-({(6-([1,1′-biphenyl]-4-yl)-4-(3,4-dimethoxyphenyl)-2*H*-1,3-oxazin-2-yl)imino}methyl)-6-methoxyphenolate lead(II) (2b):** Yield: 64%, solid brown, m.p.: 244-245 ºC. Elemental analysis for $C_{64}H_{54}N_4O_{10}Pb$ (m.w.: 1186.28) calcd. (found) %: C, 61.68 (61.16); N, 4.50 (4.45); H, 4.37 (4.36); Pb, 16.62 (16.38). Molar conductivity: 16.7 Ω^{-1} mol^{-1} cm^2.

***Bis*(-2-({(6-([1,1′-biphenyl]-4-yl)-4-(3,4,5-trimethoxyphenyl)-2*H*-1,3-oxazin-2-yl)imino}methyl)-6-methoxyphenolate lead(II) (2c):** Yield: 63%, solid dark brown, m.p.: 110 ºC. Elemental analysis for $C_{66}H_{58}N_4O_{12}Pb$ (*m.w.*: 1306.39) calcd. (found) %: C, 60.68 (60.06); N, 4.29 (4.19); H, 4.47 (4.40); Pb, 15.86 (15.80). Molar conductivity: 16.8 Ω^{-1} mol^{-1} cm^2.

***Bis*(-2-({(6-([1,1′-biphenyl]-4-yl)-4-(4-phenoxyphenyl)-2*H*-1,3-oxazin-2-yl)imino}methyl)-6-methoxyphenolate lead(II) (2d):** Yield: 63%, solid yellow, m.p.: 156-160 ºC. Elemental analysis for $C_{72}H_{54}N_4O_8Pb$ (*m.w.*: 1310.42) calcd. (found) %: C, 65.99 (64.88); N, 4.28 (4.22); H, 4.15 (4.10); Pb, 15.81 (15.78). Molar conductivity: 19.2 Ω^{-1} mol^{-1} cm^2.

***Bis*(-2-({(6-([1,1′-biphenyl]-4-yl)-4-(4-methoxyphenyl)-2*H*-1,3-thiazin-2-yl)imino}methyl)-6-methoxyphenolate lead(II) (2e):** Yield: 60%, solid dark brown, m.p.: 145-148 ºC. Elemental analysis for $C_{62}H_{50}N_4O_6S_2Pb$ (m.w.: 1218.41) calcd. (found) %: C, 61.12 (60.78); N, 4.60 (4.52); H, 4.14 (4.12); S, 5.26 (5.22); Pb, 17.01 (17.08). Molar conductivity: 18.9 Ω^{-1} mol^{-1} cm^2.

***Bis*(-2-({(6-([1,1′-biphenyl]-4-yl)-4-(3,4-dimethoxyphenyl)-2*H*-1,3-thiazin-2-yl)imino}methyl)-6-methoxyphenolate lead(II) (2f):** Yield: 67%, solid yellow, m.p.: 182-183 ºC. Elemental analysis for $C_{64}H_{54}N_4O_8S_2Pb$ (m.w.: 1278.47) calcd. (found) %: C, 60.13 (61.78); N, 4.38 (4.30); H, 4.26 (4.25); S, 5.02 (4.96); Pb, 16.21 (17.08). Molar conductivity: 22.8 Ω^{-1} mol^{-1} cm^2.

***Bis*(-2-({(6-([1,1′-biphenyl]-4-yl)-4-(3,4,5-trimethoxyphenyl)-2*H*-1,3-thiazin-2-yl)imino}methyl)-6-methoxyphenolate lead(II) (2g):** Yield: 62%, solid yellowish brown, m.p.: 282 ºC. Elemental analysis for $C_{66}H_{58}N_4O_{10}S_2Pb$ (m.w.: 1338.52) calcd. (found) %: C, 59.22 (59.01); N, 4.19 (4.09); H, 4.37 (4.36); S, 4.79 (4.70); Pb, 15.48 (15.38). Molar conductivity: 20.2 Ω^{-1} mol^{-1} cm^2.

***Bis*(-2-({(6-([1,1′-biphenyl]-4-yl)-4-(4-phenoxyphenyl)-2*H*-1,3-thiazin-2-yl)imino}methyl)-6-methoxyphenolate lead(II) (2h):** Yield: 72%, solid brown, m.p.: 199 ºC. Elemental analysis for $C_{72}H_{54}N_4O_6S_2Pb$ (m.w.: 1342.55) calcd. (found) %): C, 64.41 (64.30); N, 4.17 (4.08); H, 4.05 (4.03); S, 4.78 (4.70); Pb, 15.43 (15.00). Molar conductivity: 17.4 Ω^{-1} mol^{-1} cm^2.

Antibacterial activity: Using the disc diffusion method, all synthesized compounds were evaluated *in vitro* for antibacterial activity against Gram-positive (*S. aureus*) and Gram-negative (*E. coli*) bacteria. As a result of dissolving each lead(II) compound in DMSO, stock solutions (2 mg/mL) were prepared. Prior to sensitivity testing, bacteria were grown on Hinton-Muller agar plates and incubated at 35 ºC for 24 h. As a result, 2 mg of synthesized compounds was dissolved in 1 mL of DMSO. The solution was placed into sterile Petri plates on discs. Each bacterial strain was created in triplicate plates. For 24 h, the plates were incubated aerobically at 35 ± 2 ºC. Each molecule's antibacterial activity was compared to that of a standard antibiotic drug (streptomycin). Under the identical conditions for each organism, DMSO was employed as a negative control and a conventional antibiotic medication as a positive control. The diameter of the inhibitory zone (mm) has been used to evaluate antibacterial activity.

Docking studies: The docking programmes AutoDock Tools (ADT) 1.5.6 and AutoDock 4.2.5.1 were utilized for the molecular docking experiments. The target proteins were downloaded from the PDB database (PDB ID:3q8u). The 2D structure was converted into 3D using Chem3D Pro 12.0. MMFF94 Force field was used to minimize the energy of The MM2 force field was used to minimize the energy of oxazine and thiazine derivatives. In each iteration, the energy was reduced to the minimum root mean square gradient of 0.100. All structures were saved as pdb files for use with ADT. Grid boxes with 60 × 60 × 60 $Å^3$ dimensions and 0.375 Å spacing around the protein binding region were created using ADT [25]. The box's centre was set to the ligand centre and grid energy calculations were performed. For minimization, the hybrid Lamarckian Genetic Algorithm was used with default parameters. AutoDock tools were used to add polar hydrogen atoms, solvation parameters and Kollman unified atom type charges [26]. The docking results were examined in Discovery Studio 2020 Client.

RESULTS AND DISCUSSION

A reaction between Schiff base ligands and $Pb(CH_3COO)_2$ in solution can be described by the general eqn. 1 and **Scheme-I**:

$$Pb(OOCCH_3)_2 + 2L^{a\text{-}h}H \longrightarrow Pb(L^{a\text{-}h})_2 + 2CH_3COOH \quad (1)$$

where L = Schiff base anion. The lead complex is formed in a stoichiometric ratio of 1:2.

The lead(II) complexes were recrystallized from EtOH and obtained solid coloured compounds. At room temperature, they are extremely stable solids that do not breakdown for an extended period of time. The compound has a low hygroscopicity and is soluble in a wide variety of organic solvents. The complexes have a molar conductance of 16.00-23.00 Ω^{-1} mol^{-1} cm^2 (measured in 10^{-3} M DMSO), indicating that they are non-electrolytic.

IR spectra: IR spectra of ligands revealed a prominent band between 3450-3180 cm^{-1} attributed to ν(OH) [26] (Table-1). However, this peak is absent in the Pb(II) complexes, indicating that the phenolic oxygen has been coordinated to the lead atom *via* the loss of phenolic proton from the ligands. On complexation, a moderate strength peak at ~1278 cm^{-1} due to the ν(CO) stretching vibration is shifted to higher side, indicating the oxygen atom's participation in coordination. A moderate to strong intensity band at ~1615 cm^{-1} in the complexes may be attributed to the stretching vibration of (C=N) group [27], which first occurred in the ligands around at ~1630 cm^{-1}. The shift of this band to the lower side indicates the coordination of the azomethine nitrogen to the lead atom. The appearance of the ν(C-O) bands at a greater frequency in the IR spectra of the complexes than in those of the ligands indicates that chelation *via* phenolic oxygen reduces the repulsion between the oxygen atom's lone pair [28]. Additionally, many additional bands in the complexes found at ~560-452 cm^{-1} region could be attributed to (Pb-N)/(Pb-O) [28,29].

NMR spectra: PMR spectral analyses of ligands and their associated lead(II) complexes corroborate the above bonding pattern. The ligands' spectra include CH proton at δ 4.20 ppm and aromatic proton at δ 6.60-7.75 ppm, which resemble to the same positions in the spectra of the lead complexes. The proton of the ligands' OH group emits a signal at 12.24 ppm. This is absent from the spectra of lead complexes, indicating that the oxygen of phenolic group has chelated to lead atom. The ligand's signal at 8.85 ppm is attributable to immine protons. This signal is shifted downfield in the spectra of lead(II) complexes (9.12 ppm) as a result of its deshielding, which is a result of the immine nitrogen contributing a lone pair of electrons to the lead atom. ^{13}C NMR data for ligands and their associated lead complexes have been shown in Table-2. Carbon atoms linked to phenolic and imine groups in ligands produce signals at 156.9 and 152.3 ppm, respectively. However, these signals are visible in the spectra of lead complexes at 162.8 ppm (phenolic group) and 160 ppm (immine group) due to the coordination of the phenolic-O and azomethine-N atoms.

Frontier molecular orbital: The terms HOMO-LUMO energies have been frequently used in quantum mechanics. These orbitals have been shown to be critical in the growth of a wide variety of chemical processes and have also important for charge transfer in metal complexes [30]. The distinction between frontier and other molecular orbitals is based on the fundamental laws governing the behaviour of chemical processes. The HOMO energy is proportional to the ionization potential and indicates the molecule's vulnerability to electrophile attack. The energy of LUMO is proportional to the electron affinity of the molecule and hence indicates its sensitivity to nucleophilic attack. The HOMO and LUMO orbitals' respective energies have also been strongly linked to the ideas of hard and soft nucleophiles and electrophiles. In contrast to soft nucleophiles, hard nucleophiles have a low energy HOMO. The LUMO of hard electrophiles is higher than that of soft electrophiles and *vice versa*. The HOMO-LUMO gap is a critical measure of a molecule's kinetic stability. The LUMO-HOMO energies, hardness (η)/softness (S) and electronegativity (χ)/electrophilicity index (ω) of all synthesized compounds were computed using the B3LYP/Lanl2dz level of theory and are

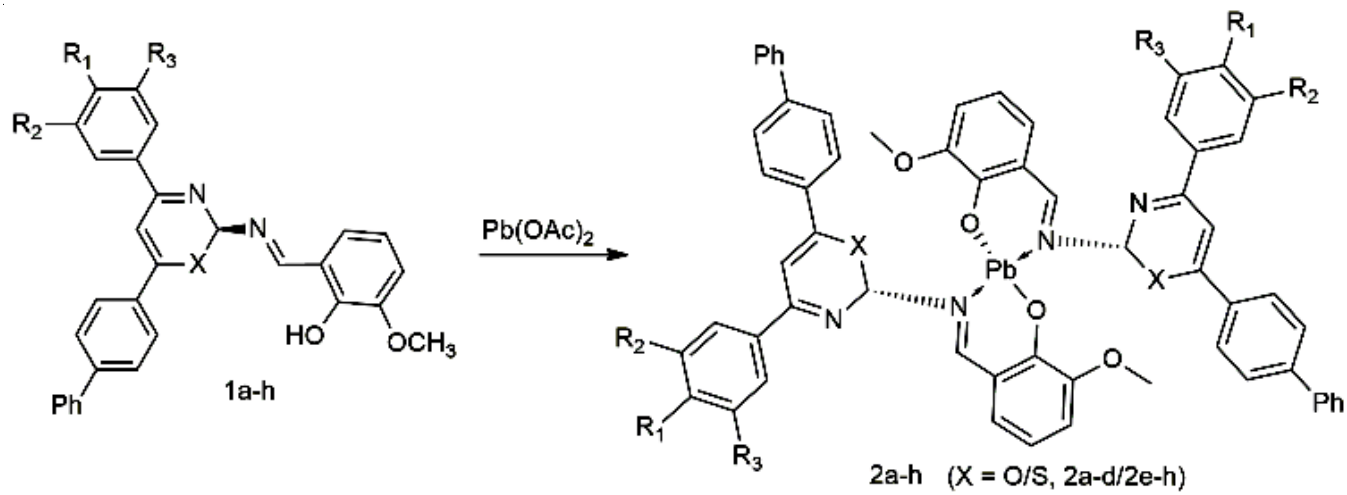

Scheme-I: Formation of lead(II) Schiff bases complexes derived from 1,3-oxazine and 1,3-thiazine derivatives

TABLE-1
KEY IR SPECTRAL BANDS (cm^{-1}) OF LEAD COMPLEXES

Compounds	Absorption band (ν, cm^{-1})					
	(Ar-H), stretching	(C=N), ring	(C=N), azomethine	(C-O)	(Pb-N)	(Pb-O)
2a	2922 m	1545 m	1614 s	1240 m	545 s	465 w
2b	2925 m	1542 m	1602 s	1260 m	540 m	460 w
2c	2932 m	1544 m	1618 m	1255 m	550 s	472 m
2d	2930 m	1558 m	1609 m	1265 m	552 s	470 m
2e	2928 m	1560 m	1625 s	1280 m	560 m	425 m
2f	2924 m	1535 m	1605 m	1278 m	565 m	430 w
2g	2934 m	1540 m	1615 s	1280 m	562 s	422 w
2h	2926 m	1532 m	1620 s	1278 m	570 s	465 m

TABLE-2
IMPORTANT NMR SPECTRAL DATA OF LEAD(II) COMPLEXES

Compounds	Chemical shift (δ ppm)	
	^{1}H NMR	^{13}C NMR
2a	(CH=N): 9.12 (s, 2H); Ar-H: 6.80-7.64 (m, 32H); oxazine (CH): 5.30 (s); αCH: 6.70 (s, 2H); OCH_3: 3.80 (s, 12H,).	165.22 (C-O), 156.28 (CH=N), 54.58 (OCH_3).
2b	(CH=N): 9.06 (s, 2H,); Ar-H: 6.82-7.66 (m, 30H); oxazine (CH): 5.32 (s); αCH: 6.76 (s, 4H); OCH_3: 3.80 (s, 18H).	162.42 (C-O), 158.28 (CH=N), 55.45 (OCH_3).
2c	(CH=N): 9.16 (s, 2H,); Ar-H: 6.80-7.72 (m, 28H); oxazine (CH): 5.30 (s); αCH: 6.72 (s, 4H); OCH_3: 3.88 (s, 24H).	160.24 (C-O), 156.82 (CH=N), 56.55 (OCH_3).
2d	(CH=N): 9.98 (s, 2H); Ar-H: 6.78-7.76 (m, 42H); oxazine (CH): 5.30 (s); αCH: 6.76 (s, 4H); OCH_3: 3.82 (s, 6H)	162.02 (C-O), 160.82 (CH=N), 56.85 (OCH_3).
2e	(CH=N): 9.06 (s, 2H); Ar-H: 6.70-7.75 (m, 32H); thiazine (CH): 5.22 (s); αCH: 6.56 (s, 4H); OCH_3: 3.80 (s, 12H)	160.42 (C-O), 164.22 (CH=N), 55.68 (OCH_3).
2f	(CH=N): 9.16 (s, 2H); Ar-H: 6.65-7.72 (m, 30H); thiazine (CH): 5.28 (s); αCH: 6.36 (s, 4H); OCH_3: 3.84 (s, 18H).	160.55 (C-O), 162.42 (CH=N), 54.56 (OCH_3).
2g	(CH=N): 9.10 (s, 2H); Ar-H 6.65-7.70 (m, 28H); thiazine (CH): 5.38 (s); αCH: 6.32 (s, 4H); OCH_3: 3.82 (s, 24H).	162.05 (C-O), 160.24 (CH=N), 55.46 (OCH_3).
2h	(CH=N): 9.12 (s, 2H); Ar-H 6.68-7.70 (m, 42H); thiazine (CH): 5.30 (s); αCH: 6.36 (s, 4H); OCH_3: 3.80 (s, 6H)	164.25 (C-O), 162.42 (CH=N), 56.54 (OCH_3).

summarized in Table-3. The small energy gap of HOMO-LUMO and high electrophilicity index of compound **2d** indicate that it has a high degree of chemical reactivity and biological activity. Figs. 1 and 2 depict the HOMO/LUMO orbital distributions of **2a**, **2d**, **2e** and **2h** compounds. The electrophilicity index values estimated for the **2a**, **2d**, **2e** and **2h** molecules were 65.800, 354.918, 34.963 and 8.091 eV, respectively. The electrophilicity index of a substance indicates how well a drug interacts with biomolecules [29].

Molecular geometries of complexes: The complex **2a** is more stable state geometries were optimized at the B3LYP/Lanl2dz without regard for symmetry, bond lengths or bond angles. Fig. 3 illustrates the optimum geometry of the lead

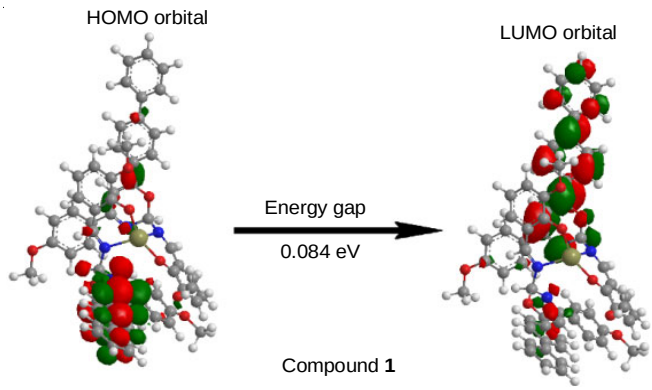

Fig. 1. HOMO-LUMO orbitals of compound **2a**

TABLE-3
CALCULATED ENERGY PARAMETERS OF LEAD(II) COMPLEXES

Parameters	Compounds							
	2a	**2b**	**2c**	**2d**	**2e**	**2f**	**2g**	**2h**
Energy (kcal/mol)	168.375	156.586	153.082	345.347	156.372	101.161	139.087	1309.74
HOMO (eV)	-4.870	-4.830	-4.905	-4.798	-4.758	-4.926	-4.923	-3.585
LUMO (eV)	-4.786	-4.455	-3.152	-4.782	-4.615	-4.878	-4.720	-3.303
Energy gap (eV)	0.084	0.375	1.753	0.016	0.143	0.048	0.203	0.282
Hardness (η)	0.042	0.1875	0.8765	0.008	0.0715	0.024	0.1015	0.141
Softness (S)	11.905	2.667	0.571	62.500	6.993	20.833	4.926	3.546
Electronegativity (χ)	-2.351	-2.040	-0.699	-2.383	-2.236	-2.415	-2.259	-1.511
Electrophilicity index (ω)	65.800	11.098	0.279	354.918	34.963	121.505	25.127	8.091

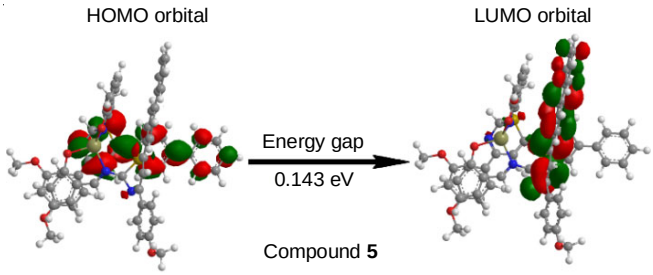

Fig. 2. HOMO-LUMO orbitals of compound **2e**

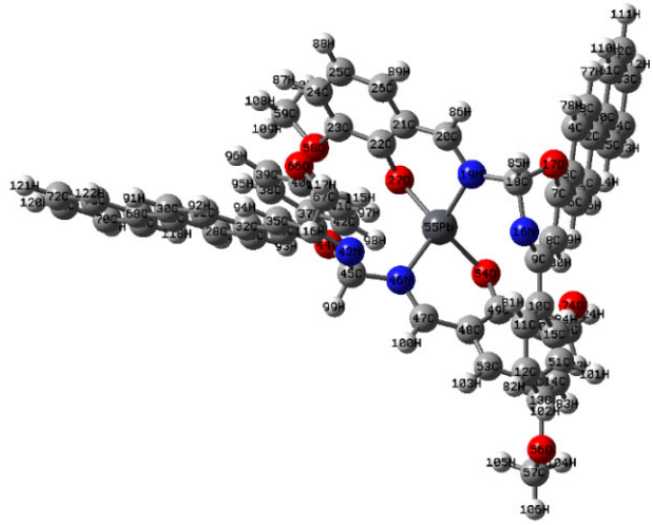

Fig. 3. Complex **2a** displayed a four-coordinate environment around lead atom by two nitrogen atoms and two oxygen atoms from two chelated ligands

complex. Table-4 lists selected geometric parameters (bond lengths and angles) for lead(II) complexes examined. Azomethine (C=N) bond lengths (C20-N19, 1.2779; C22-N46, 1.2772) are likewise enhanced by 0.0179 and 0.0172, respectively, in the complexes, in comparison to the free ligand. The observed intermediate C=N bond lengths are consistent with the occurrence of a partial double bond in the C=N bond as a result of electron delocalization during complexation. The C-O (C22-O27, 1.382; C22-O54, 1.380) bond lengths are slightly longer than those of the ligands by 0.027 and 0.025, respectively. The significant discrepancies in key bond lengths (C-O and C=N) between the ligand and lead(II) complex show that lead atom is involved in the bonding. Pb-O27 has a bond distance of 2.105/2.104 Å while Pb-O54 has a bond distance of 2.102/2.103 Å. The observed variations in Pb-O bond lengths imply the formation of Pb-O covalent/weak coordinate bonds *via* phenolic groups, respectively. The length of the lead oxygen bond is close to the total of their covalent radii (2.098). The various binding angles recorded around the lead atom range from 91.69-121.82/97.77-117.06 (Table-4). The distortions in the coordination sphere of the lead ion caused by the deformed tetrahedral geometry can be attributed to the structural limitations executed by the **2a/2e** ligands structure. Bond angles N19-Pb-O54 and N46-Pb-O27 are significantly greater in the complexes, whereas bond angles N19-Pb-O27 and N46-Pb-O27 are significantly shorter than those for a typical tetrahedral angle (109º). For compound **2a**, the optimal bond angles are 116.34º for N(19)-Pb(55)-O(54), 91.69º for N(19)-Pb(55)-O(27), 96.09º for N(46)-Pb(55)-O(54) and 113.78° for N(46)-Pb(55)-O(27). For compound **2e**, the optimal bond angles are 117.06º for the N(19)-Pb(55)-O(54) link, 97.77º for the N(19)-Pb(55)-O(27) bond, 98.04º for the N(46)-Pb(55)-O(54) bond and 113.07º for the N(46)-Pb(55)-O(27) bond. It is worth mentioning that when important bond lengths and angles from known X-ray crystal structures of lead(II) complexes are compared to those computed for **2a** and **2e**, excellent agreement is shown [30].

Antibacterial studies: The disc diffusion method was used to assess the antibacterial activity of Pb(II) compounds (**2a-h**). The chemicals were tested against *Escherichia coli* and *Staphylococcus aureus*. Antimicrobial action was demonstrated for the lead complexes against *E. coli*, a rod-shaped, aerobic, Gram-negative bacterium. *E. coli* infection can cause bloody diarrhoea and kidney failure. It causes a number of ailments, including pneumonia, septicemia, soft tissue infections, biliary tract infection, upper and lower respiratory tract infection and liver abscess. *S. aureus* is a Gram-positive spherical bacteria that can cause a variety of potentially fatal infections, including pneumonia, osteomyelitis, endocarditis and toxic shock syndrome. Toxic shock syndrome is characterized by an abrupt onset of a fever, vomiting, diarrhoea and muscle cramps, followed by hypotension, which can result in shock and death. It is possible to develop a sunburn-like rash with peeling skin.

TABLE-4
IMPORTANT BOND LENGTH (Å) AND BOND ANGLES (°) OF COMPOUNDS **2a** AND **2e**

Compound **2a**: Bond length (Å)				Compound **2a**: Bond angles (°)	
C=N	1.260	C-O	1.355	N(19)-Pb(55)-N(46)	119.18
N(19)-C(20)	1.275	C(22)-O(27)	1.382	N(19)-Pb(55)-O(54)	116.34
N(46)-C(47)	1.274	C(49)-O(54)	1.380	N(19)-Pb(55)-O(27)	91.69
N(46)-Pb(55)	2.144	O(54)-Pb(55)	2.102	N(46)-Pb(55)-O(54)	96.09
N(19)-Pb(55)	2.145	O(27)-Pb(55)	2.105	N(46)-Pb(55)-O(27)	113.78
				O(54)-Pb(55)-O(27)	121.82
Compound **2e**: Bond length (Å)				Compound **2e**: Bond angles (°)	
C=N	1.260	C-O	1.355	N(46)-Pb(55)-N(19)	116.38
N(19)-C(20)	1.278	C(22)-O(27)	1.376	N(19)-Pb(55)-O(54)	117.06
N(46)-C(47)	1.277	C(49)-O(54)	1.378	N(19)-Pb(55)-O(27)	97.77
N(46)-Pb(55)	2.145	O(54)-Pb(55)	2.103	N(46)-Pb(55)-O(54)	98.04
N(19)-Pb(55)	2.145	O(27)-Pb(55)	2.104	N(46)-Pb(55)-O(27)	113.07
				O(54)-Pb(55)-O(27)	115.60

All living species, including bacteria, replicate *via* RNA and DNA; however, many antibiotics hinder the process of DNA and RNA synthesis in bacteria, thus halting the bacteria's growth and survival. Protein synthesis is necessary for bacterial cell growth. Certain antibiotics interfere with bacterial protein synthesis by attaching to ribosome subunits, affecting normal cellular metabolism and resulting in bacterial mortality or inhibition of growth and multiplication [31]. Increased solubility of metal complexes also boosts their antibacterial action. Metal ions are absorbed by microorganisms' cell walls; these ions disturb the fungal cell's respiration process and inhibit protein synthesis, which is necessary for the organism's growth. The zone of inhibition for the investigated drugs is depicted in Fig. 4. Lead complexes of thiazines were found to have a larger zone of inhibition against bacterial strains than oxazines derivatives. Compound **2h** was found to be the most efficient against *S. aureus* and *E. coli*, exhibiting inhibition zones of 30 and 26 mm, respectively, against the test bacterial strains (Fig. 4). Lead complexes are generally more hazardous because they can act as cytotoxic species. As a result of their broad spectrum of activity, they can be employed as an antibacterial agent in the pharmaceutical sector after being examined for human toxicity.

Molecular docking: The synthesized chemicals, particularly thiazine derivatives, exhibited antibacterial action. The ligands **1h** and **2h** can be used to prevent a wide variety of disorders, ranging from minor skin infections to life-threatening diseases. The complexes' hydrophilic and hydrophobic components interact through hydrogen bonding and other electrostatic interactions. Among the docked conformations, complex **1h** exhibited the highest binding affinity (-8.18 kcal/mol), followed by complex **1d** (-7.95 kcal/mol), both of which were significantly greater than the binding affinity of traditional medicines (Table-5).

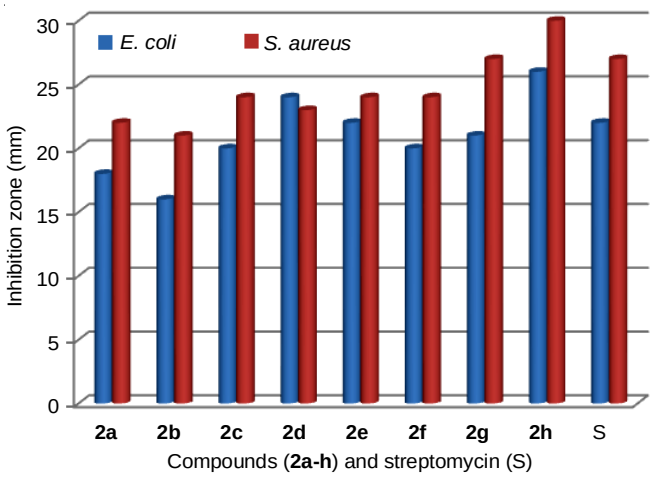

Fig. 4. Antibacterial activity of synthesized compounds **2a-h**

All the bacteria examined showed that complex **1h** is the most active compound followed by complex **1d**. These results are consistent with the antimicrobial activity results. A complete list of interactions between the NDK amino acids and **1d** and **1h** complexes and medicines is provided in Table-5. Fig. 5

TABLE-5
RESULTS OF MOLECULAR DOCKING OF THE OXAZINE AND THIAZINE DERIVATIVES ON THE ACTIVE SITE OF *Staphylococcus aureus* NUCLEOSIDE DIPHOSPHATE KINASE

Compound	Binding energy (kcal/mol)	Compound	Binding energy (kcal/mol)	Compound	Binding energy (kcal/mol)
Amoxillin	-6.45	**1a**	-6.28	**1e**	-6.90
Azithromycin	-7.83	**1b**	-7.05	**1f**	-7.55
Streptomycin	-7.61	**1c**	-7.35	**1g**	-7.91
		1d	-7.95	**1h**	-8.18

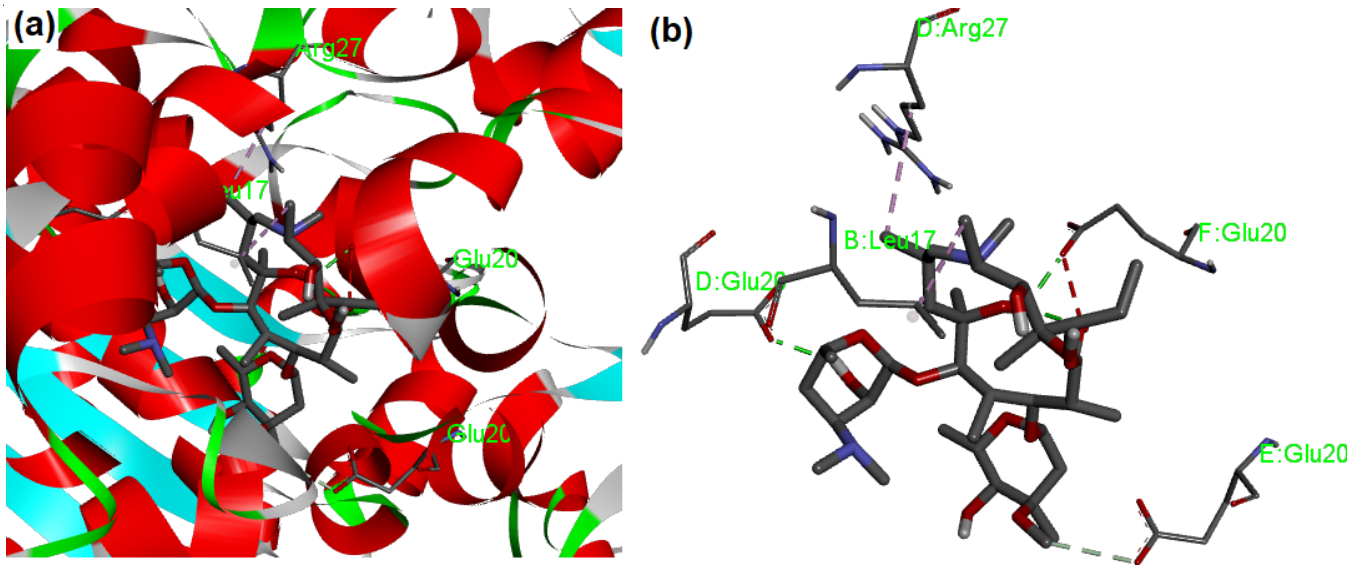

Fig. 5. Comprehensive view of *S. aureus* NDK and azithromycin after docking: (a) secondary structure of *S. aureus* NDK as a ribbon and azithromycin as a stick model and coloured according to elements. (b) interactions between azithromycin and NDK amino acids

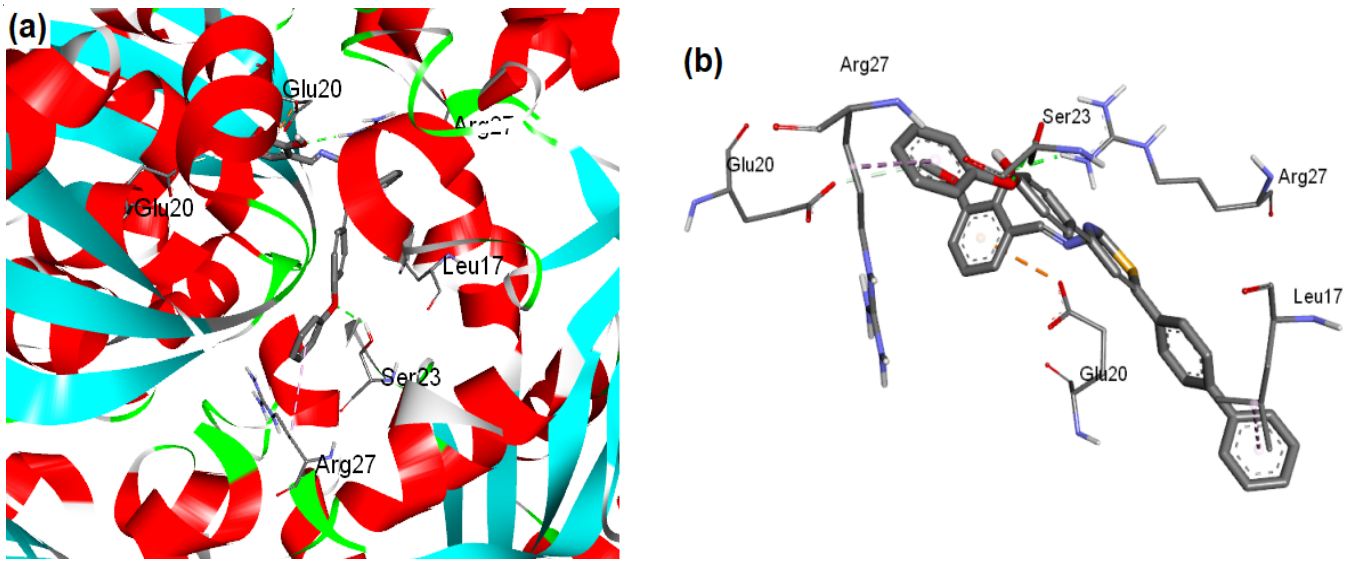

Fig. 6. Comprehensive view of *S. aureus* NDK and compound **1h** after docking: (a) secondary structure of *S. aureus* NDK as a ribbon and compound **1h** as a stick model and coloured according to elements. (b) interactions between compound **1h** and NDK amino acids

shows that azithromycin has just hydrogen bond interactions, but compound **1h** (Fig. 6) has hydrophobic as well as electrostatic interactions, resulting in a greatly higher binding affinity for azithromycin. In Fig. 6, compound **1h** forms steric interaction with active amino acids *viz.* Glu 20, Arg 27, Ser 23 and Leu 17, which helps in binding of compound **1h** at active site as similar to the azithromycin.

Conclusion

Lead(II) compounds of Schiff bases obtained from oxazine and thiazine derivatives were synthesized and characterized. Ligands LH (**1a-h**) were covalently linked to Pb(II) ions *via* oxygen and nitrogen atoms to form the appropriate complexes. Different microanalytical and spectroscopic approaches, as well as DFT computations, have been used to analyze synthesized Pb(II) complexes. All the Pb(II) complexes possessed distorted tetrahedral geometry and were four-coordinated. A preliminary *in vitro* antibacterial research revealed that all the Pb(II) complexes developed had a high level of activity against the tested bacterial strains and was somewhat more active than the standard. Docking studies showed that the binding mode of the thiazine derivatives is comparable to oxazine and superior to azithromycin. *S. aureus*' susceptibility to these compounds highlights the importance of further research into their antibacterial activity.

ACKNOWLEDGEMENTS

The authors thanks to the Dean, School of Liberal Arts and Science, Mody University of Science and Technology, Lakshmangarh (Sikar), India, for providing the research facilities.

CONFLICT OF INTEREST

The authors declare that there is no conflict of interests regarding the publication of this article.

REFERENCES

1. P. Modak, W. Hammond, M. Jaffe, M. Nadig and R. Russo, *J. Appl. Polym. Sci.*, **137**, 49756 (2020); https://doi.org/10.1002/app.49756
2. E. Raczuk, B. Dmochowska, J. Samaszko-Fiertek and J. Madaj, *Molecules*, **27**, 787 (2022); https://doi.org/10.3390/molecules27030787
3. A. Kajal, S. Bala, S. Kamboj, N. Sharma and V. Saini, *J. Catal.*, **2013**, 893512 (2013); https://doi.org/10.1155/2013/893512
4. A.K. Varshney, S. Varshney, M. Sharma and H.L. Singh, *Phosphorus Sulfur Silicon Rel. Elem.*, **161**, 163 (2000); https://doi.org/10.1080/10426500008042104
5. H. ElGhamry, N. El-Wakiel and A. Khamis, *Appl. Organomet. Chem.*, **32**, e4583 (2018); https://doi.org/10.1002/aoc.4583
6. S. Sarkar, M. Jana, T. Mondal and C. Sinha, *J. Organomet. Chem.*, **716**, 129 (2012); https://doi.org/10.1016/j.jorganchem.2012.06.009
7. N. Turan, *J. Electron. Mater.*, **48**, 7366 (2019); https://doi.org/10.1007/s11664-019-07562-3
8. V.S.V. Rani, T. Dhanasekaran, M. Jayathuna, V. Narayanan and D. Jesudurai, *Mater. Today Proc.*, **5**, 8784 (2018); https://doi.org/10.1016/j.matpr.2017.12.306
9. M.K. Ghosh, S. Pathak and T.K. Ghorai, *ACS Omega*, **4**, 16068 (2019); https://doi.org/10.1021/acsomega.9b02268
10. S. Shaygan, H. Pasdar, N. Foroughifar, M. Davallo and F. Motiee, *Appl. Sci.*, **8**, 385 (2018); https://doi.org/10.3390/app8030385
11. M.A. Malik, O.A. Dar, P. Gull, M.Y. Wani and A.A. Hashmi, *MedChemComm*, **9**, 409 (2018); https://doi.org/10.1039/C7MD00526A
12. H.L. Singh, J.B. Singh and S. Bhanuka, *J. Assoc. Arab Univ. Basic Appl. Sci.*, **23**, (2017); https://doi.org/10.1016/j.jaubas.2016.05.003
13. A. Reiss, N. Cioaterã, A. Dobritescu, M. Rotaru, A.C. Carabet, F. Parisi, A. Gănescu, I. Dăbuleanu, C.I. Spînu and P. Rotaru, *Molecules*, **26**, 3062 (2021); https://doi.org/10.3390/molecules26103062
14. S.N. Sovari and F. Zobi, *Chem. Eur. J.*, **2**, 418 (2020); https://doi.org/10.3390/chemistry2020026
15. S.E.A. El-Razek, S.M. El-Gamasy, M. Hassan, M.S. Abdel-Aziz and S.M. Nasr, *J. Mol. Struct.*, **1203**, 127381 (2020); https://doi.org/10.1016/j.molstruc.2019.127381

16. E. Peterson and P. Kaur, *Front. Microbiol.*, **9**, 2928 (2018); https://doi.org/10.3389/fmicb.2018.02928
17. M.J. Cheesman, A. Ilanko, B. Blonk and I.E. Cock, *Pharmacogn. Rev.*, **11**, 57 (2017); https://doi.org/10.4103/phrev.phrev_21_17
18. A.R.M. Coates and Y. Hu, *Br. J. Pharmacol.*, **152**, 1147 (2007); https://doi.org/10.1038/sj.bjp.0707432
19. A. Evans and K.A. Kavanagh, *J. Med. Microbiol.*, **70**, 001363 (2021); https://doi.org/10.1099/jmm.0.001363
20. E. Lionta, G. Spyrou, D.K. Vassilatis and Z. Cournia, *Curr. Top. Med. Chem.*, **14**, 1923 (2014); https://doi.org/10.2174/1568026614666140929124445
21. P. Szymański, M. Markowicz and E. MikiciukOlasik, *Int. J. Mol. Sci.*, **13**, 427 (2011); https://doi.org/10.3390/ijms13010427
22. R.J. Henry, *Bacteriol. Rev.*, **7**, 175 (1943); https://doi.org/10.1128/br.7.4.175-262.1943
23. M.J. Frisch, G.W. Trucks, H.B. Schlegel, G.E. Scuseria, M.A. Robb, J.R. Cheeseman, J.A. Montgomery, Jr., T. Vreven, K.N. Kudin, J.C. Burant, J.M. Millam, S.S. Iyengar, J. Tomasi, V. Barone, B. Mennucci, M. Cossi, G. Scalmani, N. Rega, G.A. Petersson, H. Nakatsuji, M. Hada, M. Ehara, K. Toyota, R. Fukuda, J. Hasegawa, M. Ishida, T. Nakajima, Y. Honda, O. Kitao, H. Nakai, M. Klene, X. Li, J.E. Knox, H.P. Hratchian, J.B. Cross, V. Bakken, C. Adamo, J. Jaramillo, R. Gomperts, R.E. Stratmann, O. Yazyev, A.J. Austin, R. Cammi, C. Pomelli, J.W. Ochterski, P.Y. Ayala, K. Morokuma, G.A. Voth, P. Salvador, J.J. Dannenberg, V.G. Zakrzewski, S. Dapprich, A.D. Daniels, M.C. Strain, O. Farkas, D.K. Malick, A.D. Rabuck, K. Raghavachari, J.B. Foresman, J.V. Ortiz, Q. Cui, A.G. Baboul, S. Clifford, J. Cioslowski, B.B. Stefanov, G. Liu, A. Liashenko, P. Piskorz, I. Komaromi, R.L. Martin, D.J. Fox, T. Keith, M.A. Al-Laham, C.Y. Peng, A. Nanayakkara, M. Challacombe, P.M.W. Gill, B. Johnson, W. Chen, M.W. Wong, C. Gonzalez and J.A. Pople, Gaussian, Inc., Wallingford CT (2004).
24. A. Sharma, S. Khaturia and H.L. Singh, *Asian J. Chem.*, **33**, 531 (2021); https://doi.org/10.14233/ajchem.2021.23050
25. M. Mansourian, A. Fassihi, L. Saghaie, A. Madadkar-Sobhani, K. Mahnam and M. Abbasi, *Med. Chem. Res.*, **24**, 394 (2015); https://doi.org/10.1007/s00044-014-1133-7
26. G.M. Morris, R. Huey, W. Lindstrom, M.F. Sanner, R.K. Belew, D.S. Goodsell and A.J. Olson, *J. Comput. Chem.*, **30**, 2785 (2009); https://doi.org/10.1002/jcc.21256
27. H.L. Singh, J. Singh and A. Mukherjee, *Bioinorg. Chem. Appl.*, **2013**, 425832 (2013); https://doi.org/10.1155/2013/425832
28. H.L. Singh, J.B. Singh and H. Sachedva, *Spectrosc. Lett.*, **46**, 286 (2013); https://doi.org/10.1080/00387010.2012.700545
29. H.L. Singh, S.S. Chauhan and H. Sachedva, *Res. Chem. Intermed.*, **36**, 1037 (2010); https://doi.org/10.1007/s11164-010-0216-4
30. S. Bhanuka and H.L. Singh, *Rasayan J. Chem.*, **10**, 673 (2017); https://doi.org/10.7324/RJC.2017.1021668
31. M.R. Yeaman and N.Y. Yount, *Pharmacol. Rev.*, **55**, 27 (2003); https://doi.org/10.1124/pr.55.1.2